Electronic Supplementary Material (ESI) for Soft Matter.

Supporting Information

Multicompartment calcium alginate microreactors to reduce substrate inhibition in enzyme cascade reactions

*Yongkang Xi,[a] Bradley D. Frank,[a] Apostolos Tatas,[a] Marko Pavlovic,[a,b] and Lukas Zeininger[a,]**

[a] Department of Colloid Chemistry, Max Planck Institute of Colloids and Interfaces, Am Muehlenberg 1, 14476 Potsdam, Germany;

* corresponding author e-mail: lukas.zeininger@mpikg.mpg.de

[b] Department of Physics and John A. Paulson School of Engineering and Applied Sciences, Harvard University, Cambridge, Massachusetts, 02138, USA

Table of Contents

Supporting Figures

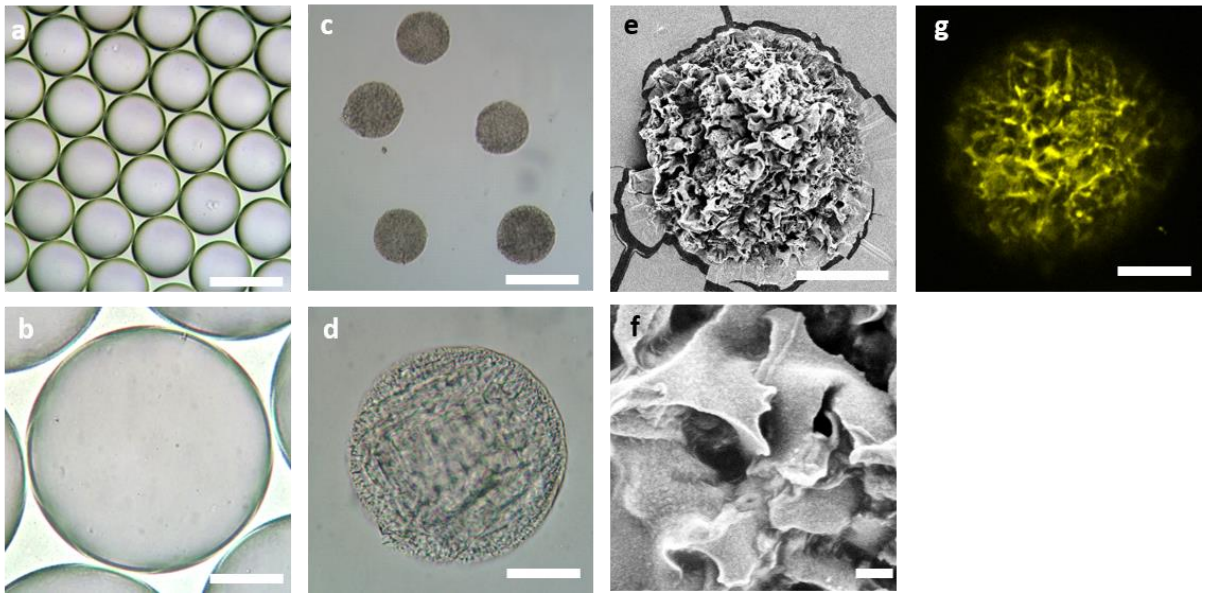

Figure S1. Microscopic characterization of single-phase hydrogel particles prepared using the freeze thaw approach. a) Optical micrograph of the alginate-containing aqueous emulsion precursors prepared using microfluidic methods; scale bar: 200 µm; b) magnification of the droplet template in a, scale bar: 50 µm; c) Optical micrographs of corresponding hydrogel particles formed via gelation of the droplet precursors shown in a and b, scale bar: 200 µm; d) magnification of the hydrogel particles shown in c, scale bar: 50 µm; e) SEM of a dried Ca-alginate hydrogel particle, scale bar: 10 µm; f) magnification of the latter showing the surface roughness of the dried Ca-alginate hydrogel particle, scale bar: 1 µm; g) Fluorescence micrograph of Ca-alginate hydrogel particle prepared using FITC labeled alginate, scale bar: 50 µm.

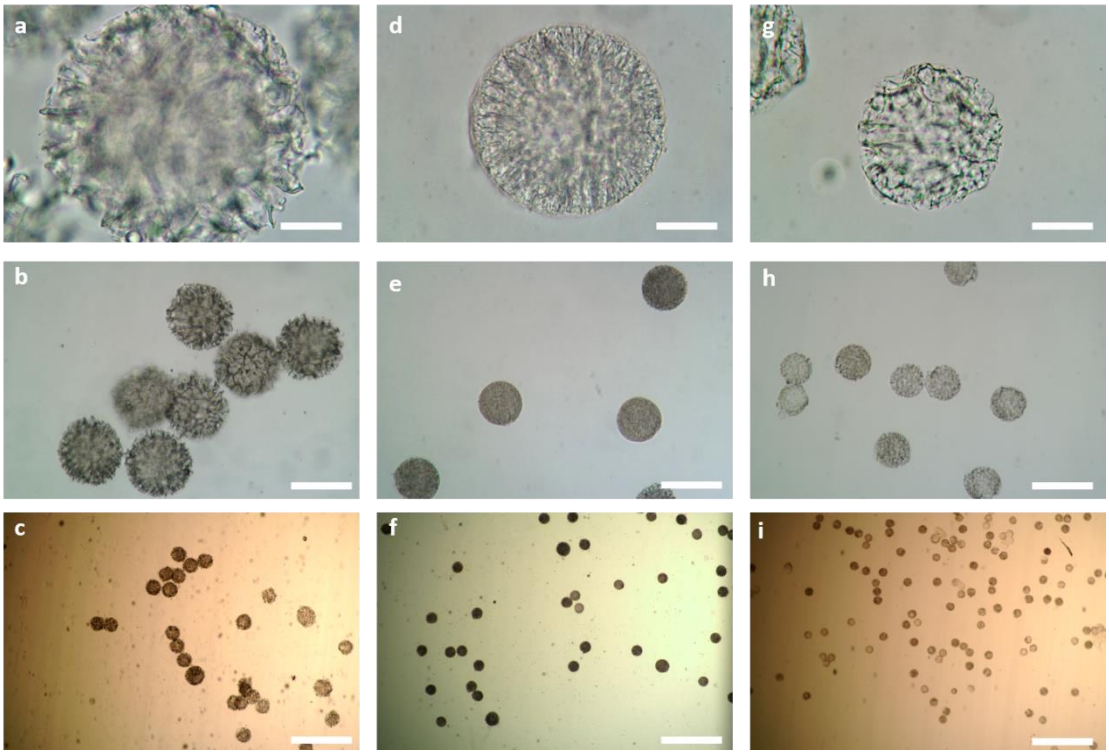

Figure S2. Micrographs of differently sized single phase Ca-alginate hydrogel particles prepared using droplet templates of different sizes. The different micrographs display particles at different sizes prepared using the freeze thaw approach by varying the size of the droplet precursors via controlling the flow rate in the microfluidic channels. The micrographs display large particles with a diameter of d= 208.96 µm ± 1.91 µm (a-c), medium sized particles with a diameter of d= 53.92 µm ± 1.96 µm (d-f), and small hydrogel particles with a diameter of d= 112.75 µm ± 7.19 µm (g-i) at different magnification. Scale bar: top row: 50 µm, middle row: 200 µm, bottom row: 1000 µm.

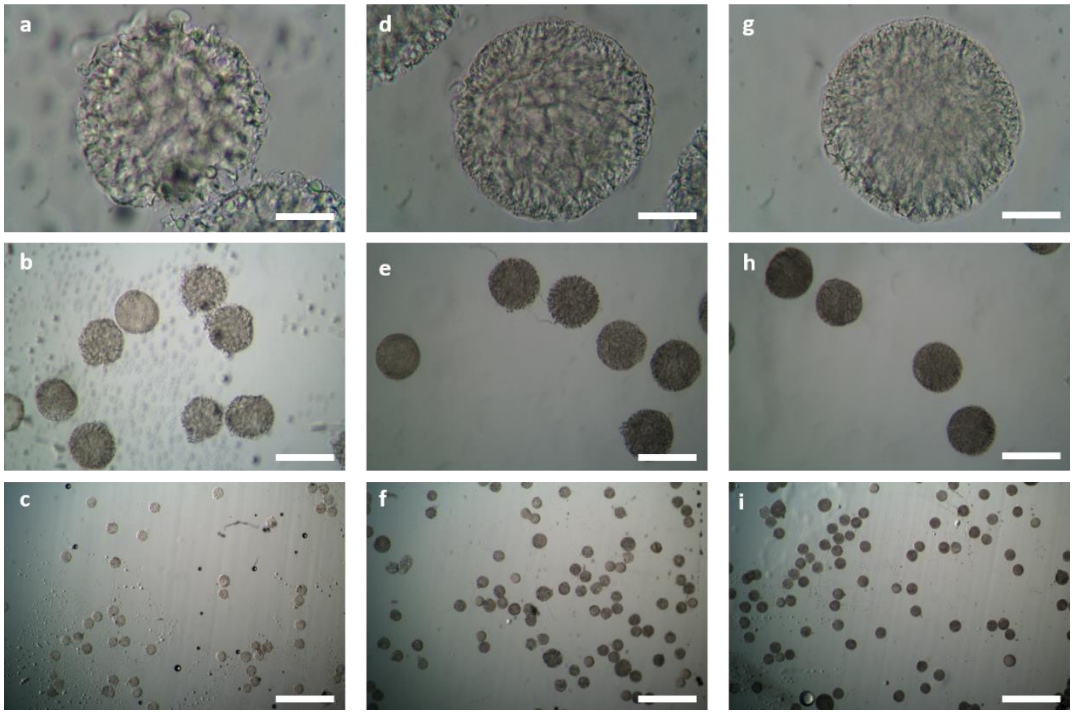

Figure S3. Single phase Ca-alginate hydrogel particles prepared inside differently concentrated CaCl2 solutions. For all particles, droplet precursors contained 2.5 wt. % alginate. The micrographs display particles prepared inside aqueous solutions containing Ca^{2+} at concentrations of 80mM (a-c), 160mM (d-f) 240mM (g-i), Scale bar: top row: 50µm middle row: 200µm and bottom row: 1000µm.

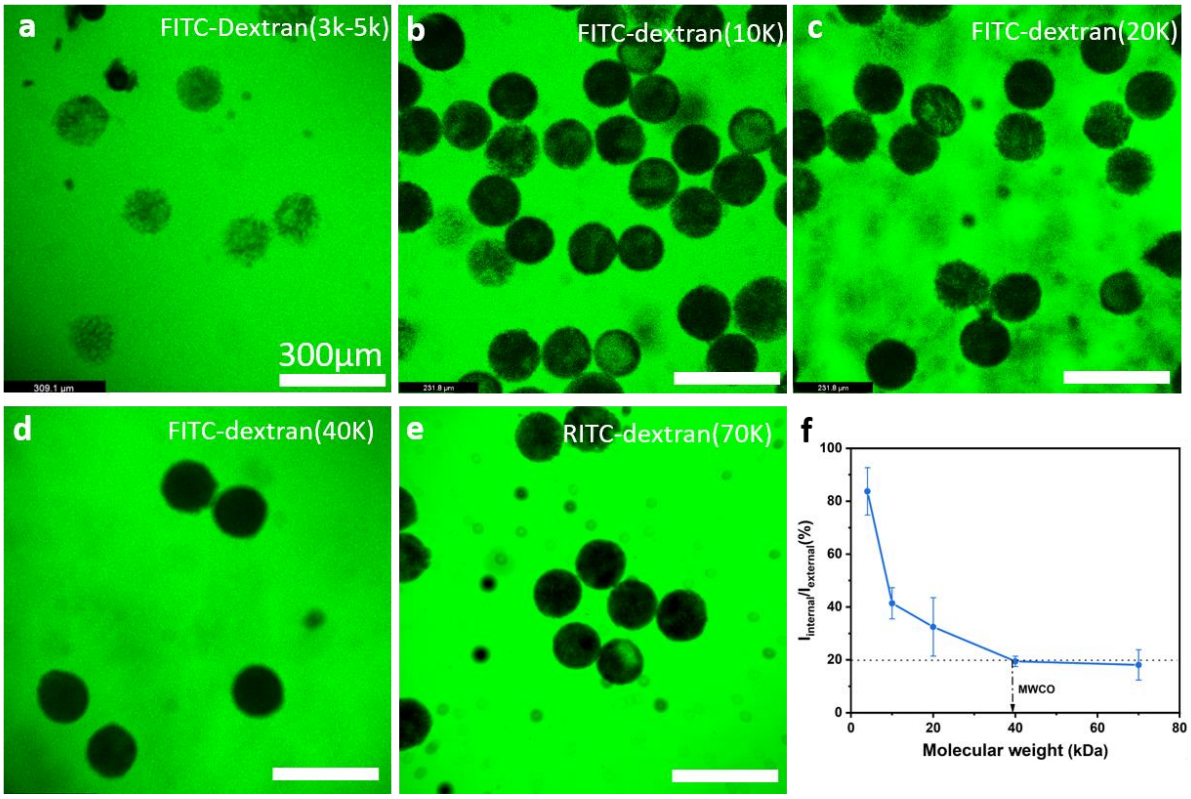

Figure S4. Investigation of the semi-permeability of synthesized hydrogel particles and determination of the molecular weight cut off (MWCO). a-e)Fluorescence micrographs of Ca-alginate hydrogel particles exposed to FITC or RITC-labeled dextran of different molecular weights; f) Plot of the fluorescence intensity ratio of the fluorescence from labeled dextrans in the continuous phase to the fluorescence intensity on the inside of the particles as a function of the molecular weight of the dextran. The graph reveals the molecular weight cut-off MWCO = 40 kDa, above which 80 % of the solute is retained by the hydrogel particles.

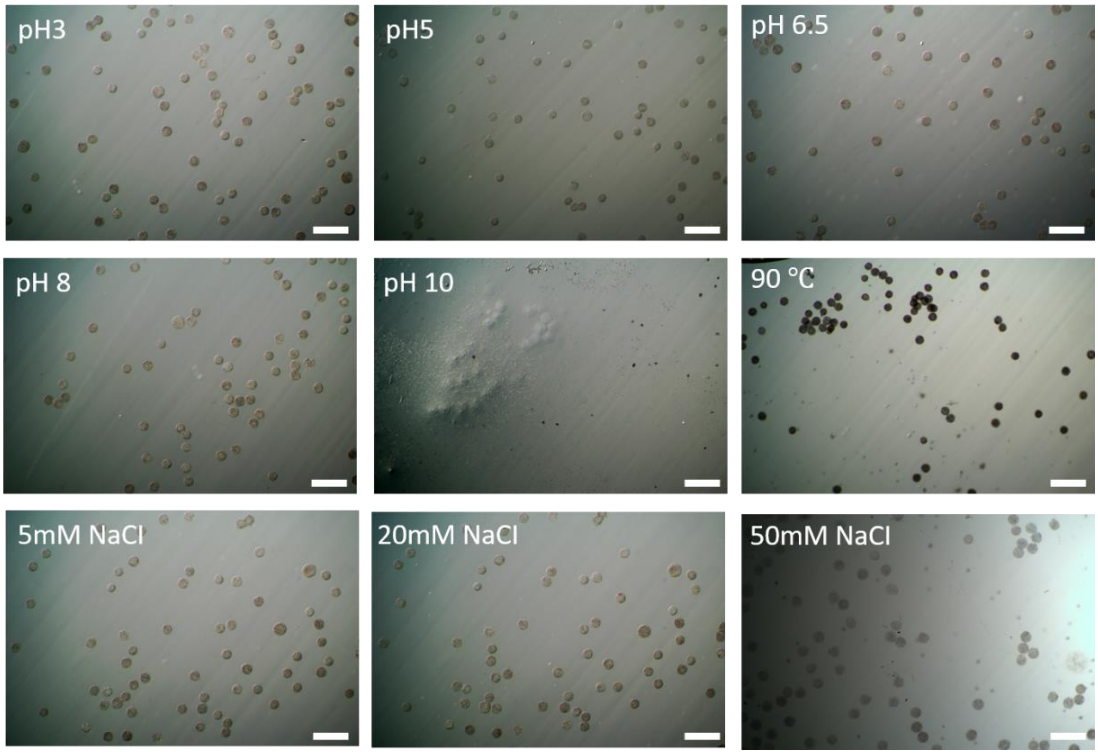

Figure S5. Test of hydrogel particle stability to variations in external conditions. Micrographs depict pristine single-phase particles, after 30 min of exposure to aqueous solutions of hydrochloric acid or sodium hydroxide at pH = 3, 5, 6.5, 8, and 10, after 30 min at elevated temperature of T = 90°C, and after 30 min exposure to aqueous NaCl solutions at concentrations of 5mM, 20 mM, and 50 mM. scale bar: 500 µm.

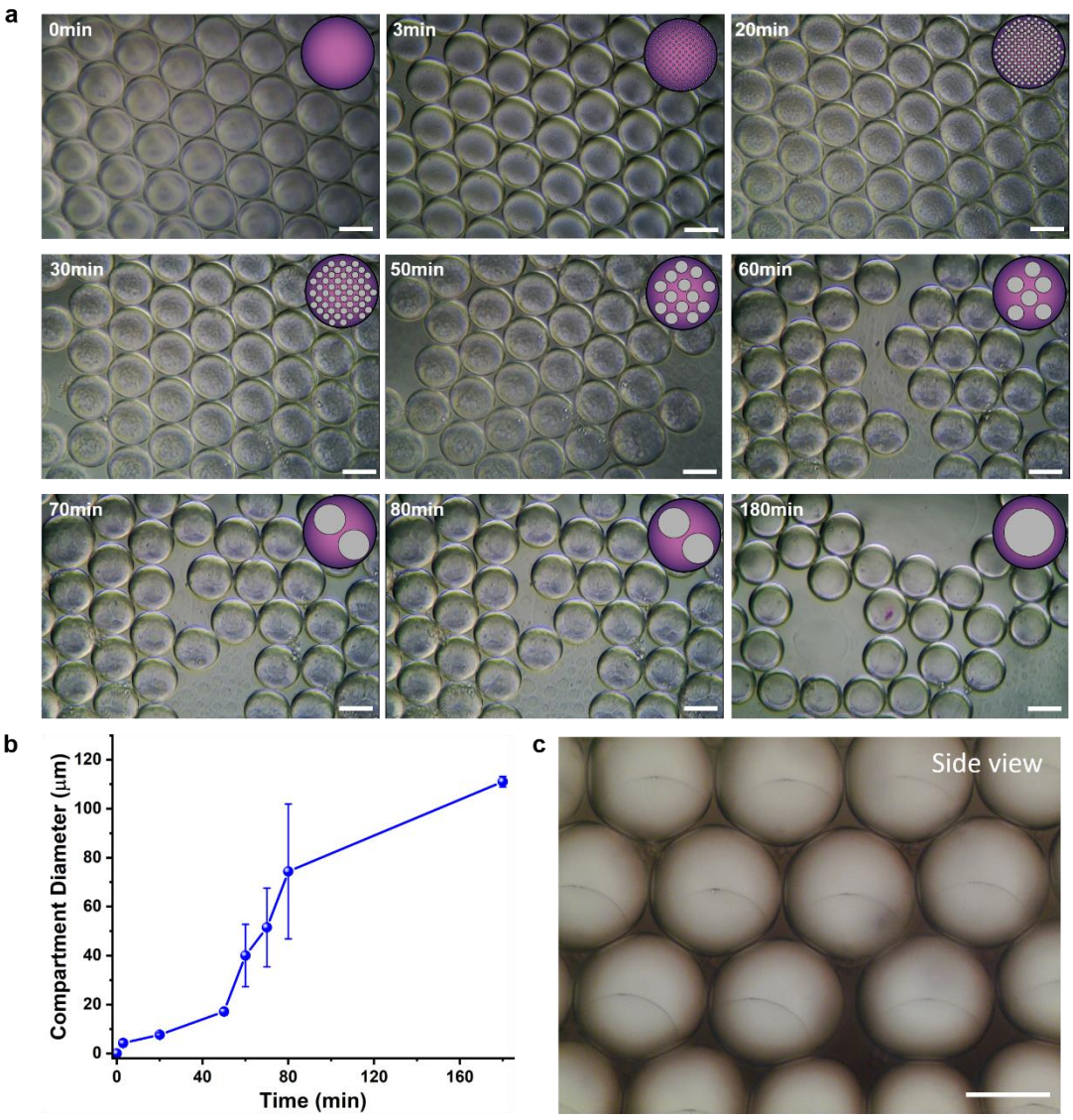

Figure S6. Optical micrographs of the time-dependent progress of liquid-liquid phase-separation inside aqueous droplets consisting of PEG (MW: 35 kDa), dextran (MW: 500 kDa) and alginate (2.5 wt.%) induced via placing droplets generated at elevated temperatures at room temperature. (a) The top view optical micrographs depict the time-dependent progress of phase-separation by first forming highly multicompartmentalized droplets containing many small dextran-rich compartments that then merge into larger droplets and ultimately form Janus droplets comprised of two distinct hemispheres; scale bar: 100 μm; (b) Plot of time-dependent increase in the compartment diameter of a droplet with a diameter of 130 μm; (c) Side-view optical micrograph of the droplets after complete phase separation; scale bar: 100 μm.

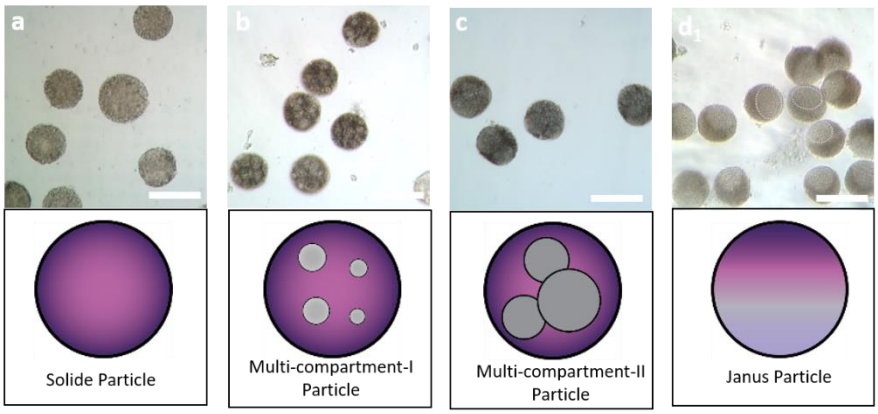

Figure S7. Optical micrographs of compartmentalized hydrogel particles. Obtained hydrogel particles after the gelation of droplet templates comprised of 2.5 wt.% sodium alginate, 1.8 wt.% PEG35kDa and 3.3 wt.% dextran 500kDa after phase-separation at room temperature for 0 min, 20 min, 40 min and 180 min; scale bar: 200 µm.

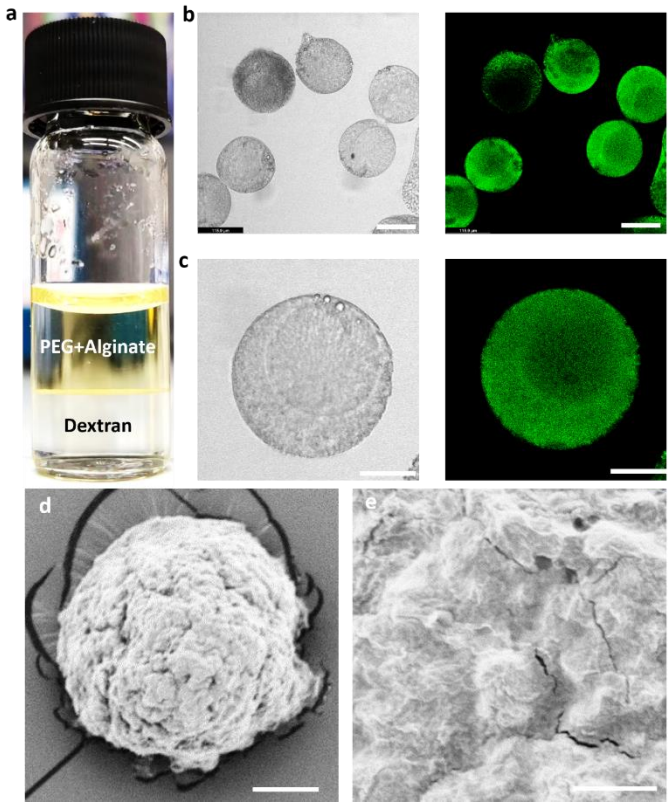

Figure S8. Characterization of Ca-alginate hydrogel Janus particles. a) Image of the bulk ATPS (V = 4 mL) displaying the predominant FITC-labeled alginate partitioning into the PEG-rich phase via yellow staining of the respective ATPS phase; b-c) Optical bright field (left) and fluorescence (right) micrographs of hydrogel Janus particles displaying the different crosslinking density of Ca-alginate (labeled with FITC) in the two phases due to the preferred partitioning of alginate into the PEG-rich phase of the droplet precursors; scale bars: 100 µm for b and 50 µm for c; d-e) SEM images of dried hydrogel Janus particles; scale bar: 20 µm for d and 2 µm for e.

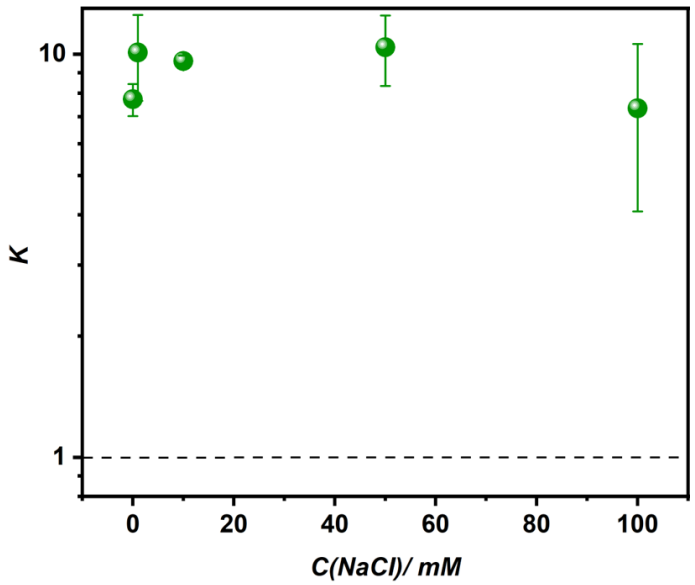

Figure S9. Determination of the partitioning coefficient (K) of catalase. Partitioning coeffiecients of catalase inside an ATPS comprised 2.5 wt.% sodium alginate, 1.82 wt.% PEG 35K, and 3.63 wt.% dextran 500K containing different concentrations of NaCl. Enzyme concentrations in the manually separated top and bottom phases of the ATPS were determined by performing the Bradford test.

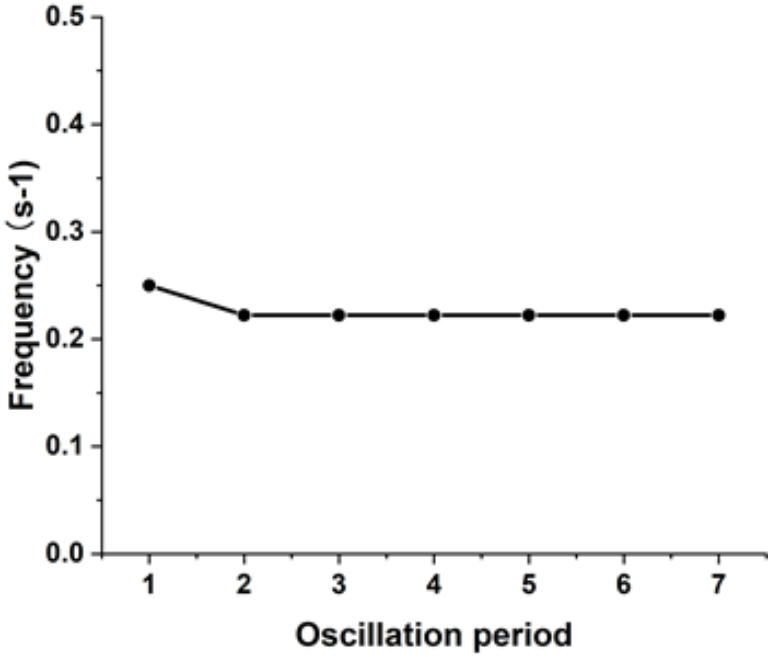

Figure S10. Oscillation frequency of catalase-functionalized hydrogel particles during the first 7 cycles.

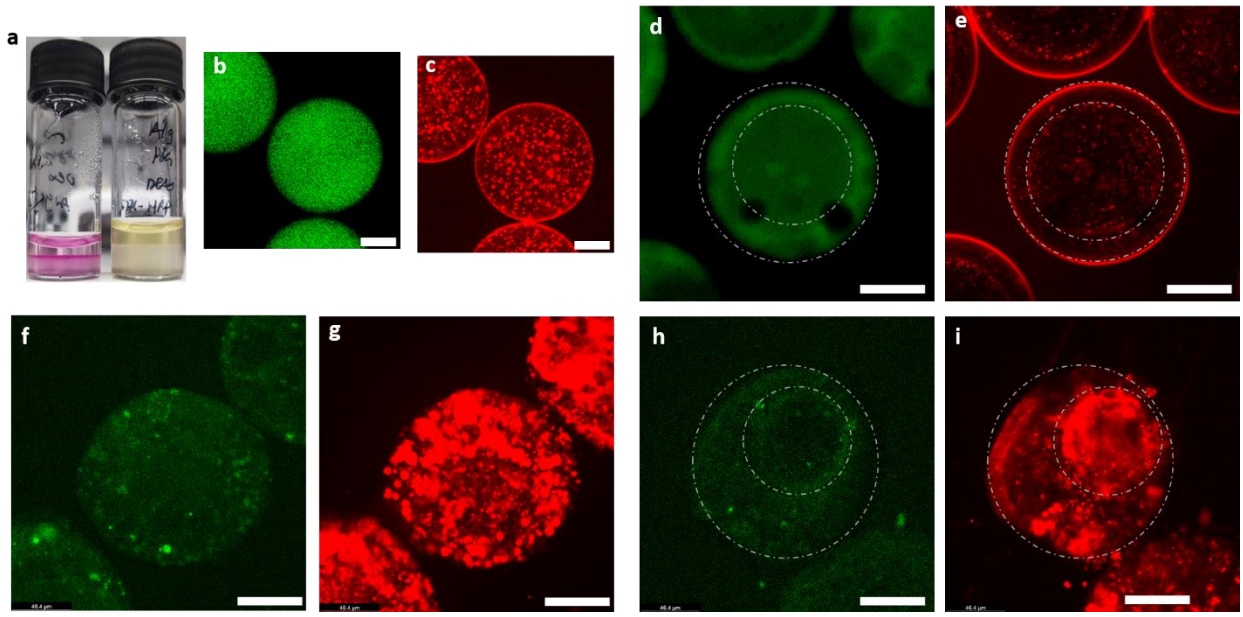

Figure S11. Visualization of HRP and GOX enzyme cross-partitioning inside droplets and corresponding hydrogel particles. a) Visualization of preferential FITC-labeled HRP and RITC-labeled GOX partitioning into the opposite phases of a bulk ATPS comprised of PEG 35k and dextran 500k through different staining of the two phases; b,c) Fluorescence micrographs showing the different partitioning of the two enzymes inside multi-compartmentalized (b,c) and Janus droplets (d,e). Droplets contained both FITC-labeled HRP and RITC-labeled GOX. Selective excitation of the two fluorophores indicates differences in the relative phase-preferential localization of the enzymes; f-i) Fluorescence micrographs of hydrogel particles obtained after gelation of the droplet precursors displayed in b-e. A direct comparison of the green vs. red fluorescence intensity distributions throughout the particles indicates differences in the phase-preferential partitioning of the two enzymes. All scale bars: 50 µm.

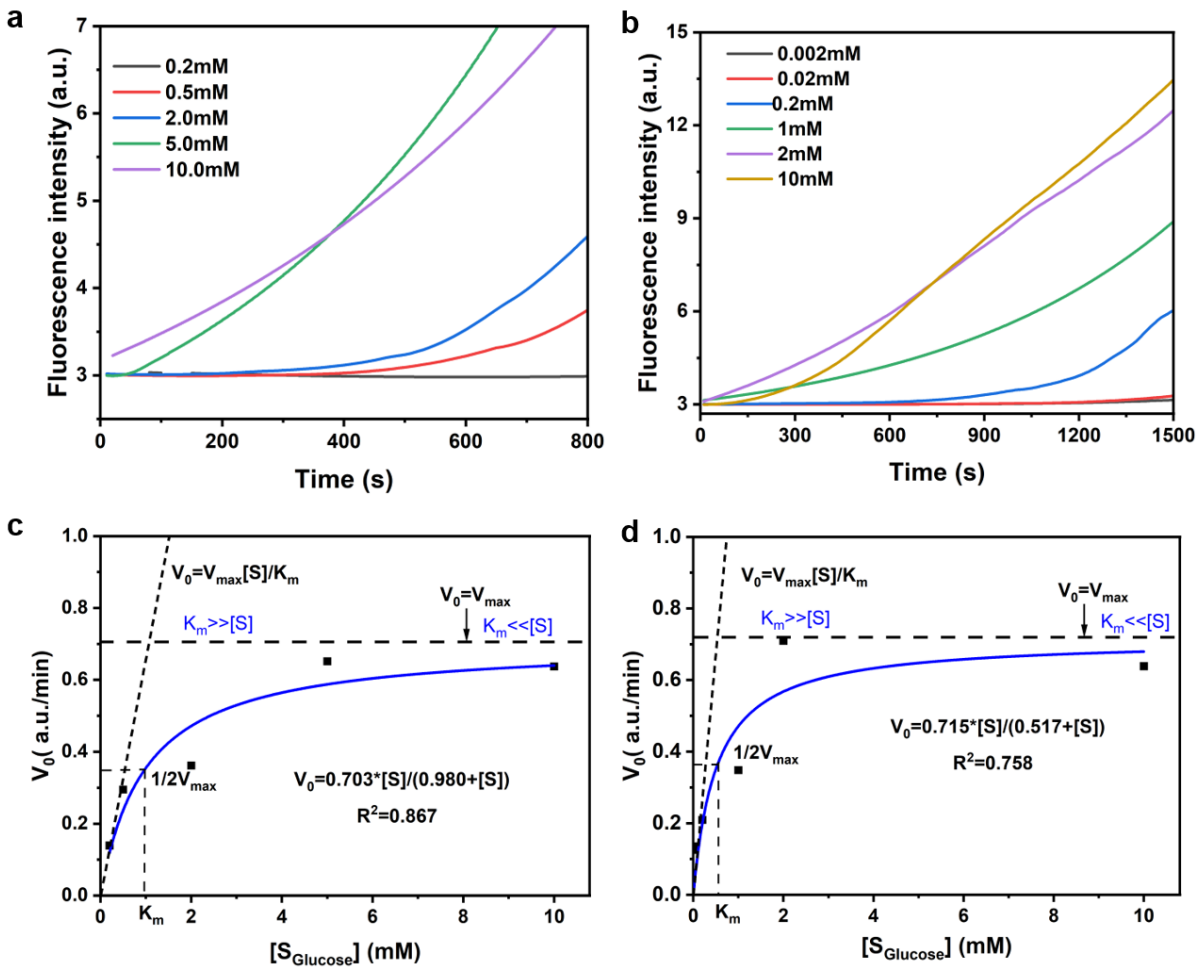

Figure S12. Determination of the Michaelis-Menten constant and maximum reaction velocity of the cascade reaction. a) Time-dependent increase in fluorescence intensity stemming from the cascade reaction product resorufin as a function of different added glucose concentrations inside multi-compartmentalized hydrogel particles with low phase-preferential partitioning of the two enzymes HRP and GOX; b) Same time-dependent evolution of the cascade reaction for particles containing cross-compartmentalized enzymes as controlled via modulating the salt concentration inside the respective droplet precursors; c-d) Plot of the initial reaction velocity versus glucose concentration for the determination of the maximum reaction velocity and Michaelis Menten constant for the two different systems (multicompartmentalized hydrogel particles with almost uniform enzyme distribution throughout both phases (c) and phase-preferential partitioning of the two enzymes (d)). Values for K_m and V_{max} were obtained by fitting the experimental data using the Micahelis-Menten equation $V_0 = \frac{V_{max}*[S]}{K_m+[S]}$, where V_0 is the initial reaction velocity and [S] the glucose concentration at the beginning of the cascade reaction.

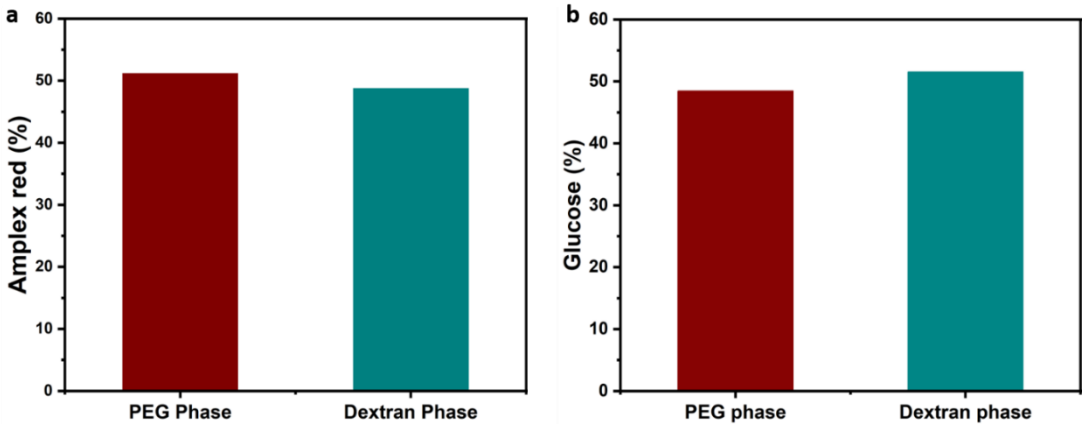

Figure S13. Partitioning behavior of the cascade reaction substrates. The relative partitioning of the substrates of the enzyme cascade reaction was determined via addition of the substrates glucose (100 mM) or amplex red (2 mM), respectively, to a bulk ATPS solution (1 mL) prior to separating the two phases. Initiation of the enzyme cascade via addition of the enzymes HRP and GOX resulted in the formation of the fluorescent marker resorufin and the relative fluorescence intensity of the individual phases was recorded.

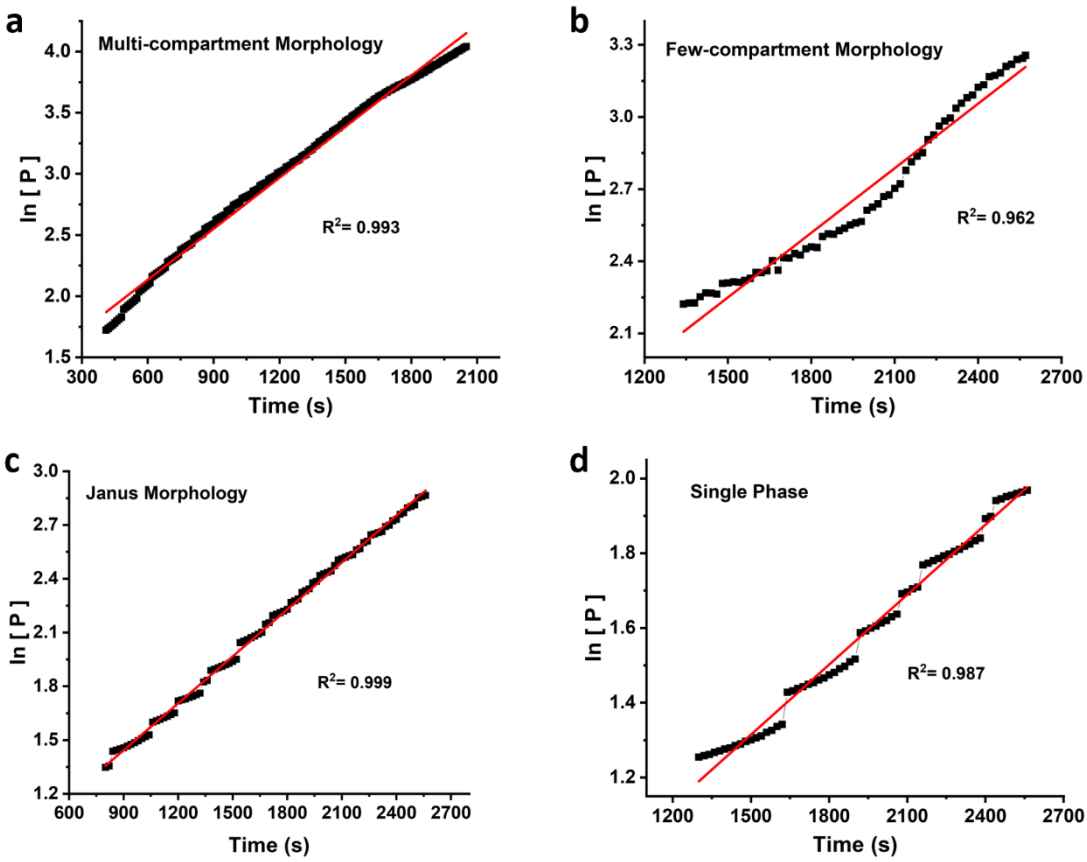

Figure S14. Determination of the morphology dependent reaction rate of the enzyme cascade. Determination of the pseudo-first order reaction constants for cascade reaction inside differently compartmentalized hydrogel particle structures, (a) Multi-compartment morphology, (b) few-compartment morphology, (c) Janus morphology and (d) single phase particles.

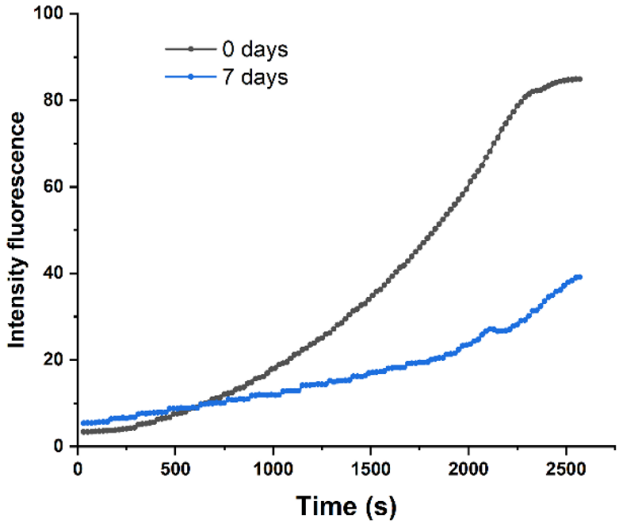

Figure S15. Stability of enzyme-containing hydrogel particles. Time-dependent catalytic activity of enzyme (HRP, GOX) containing multi-compartment particles.

Table S1. Enzyme encapsulation efficiency of hydrogel particles in different morphologies. The concentration of the encapsulated enzyme was calculated by determining the protein concentration in the bulk solution. To this end, hydrogel particles were subjected to centrifugation and subsequently washed three times using deionized water. The aqueous supernatants were collected and combined and the detection of the free enzyme content in the bulk solution was determined using Bradford's method. The tabulated data below presents the outcomes of these experiments, indicating that there is minimal variation in the protein concentration within hydrogel particles of diverse geometries (Table S1).

Particle Type	Enzyme concentration	Encapsulation efficiency
Single phase particles	1.93mg/g	96.74%
Janus morphology	1.95 mg/g	97.60%
Few-compartment morphology	1.97 mg/g	98.47%
Multi-compartment morphology	1.96 mg/g	98.18%